

Temporal Evolution of the Radial Distribution of Milky Way Satellite Galaxies

EKTA PATEL ^{1,*} LIPIKA CHATUR ² AND YAO-YUAN MAO ¹

¹*Department of Physics and Astronomy, University of Utah, 115 South 1400 East, Salt Lake City, Utah 84112, USA*

²*Department of Astronomy, The University of Texas at Austin, 2515 Speedway Boulevard, Austin, TX 78712, USA*

(Accepted October 15, 2024)

ABSTRACT

The Milky Way (MW) is surrounded by dozens of satellite galaxies, with six-dimensional (6D) phase space information measured for over 80% of this population. The spatial distribution of these satellites is an essential probe of galaxy formation and for mapping the MW’s underlying dark matter distribution. Using measured 6D phase space information of known MW satellites, we calculate orbital histories in a joint MW+LMC potential, including the gravitational influence of the LMC on all satellites, on the MW’s center of mass, and dynamical friction owing to both galaxies, to investigate the evolution of the MW’s cumulative radial profile. We conclude radial profiles become more concentrated over time when we consider the LMC’s gravitational influence and the group infall of LMC-associated satellites. The MW’s radial distribution is consistently more concentrated at present-day, 1 Gyr, and 2 Gyr ago compared to recent surveys of nearby MW-like systems. Compared to MW-mass hosts in cosmological, zoom-in simulations, we find the MW’s radial profile is also more concentrated than those of simulated counterparts; however, some overlap exists between simulation results and our analysis of the MW’s satellite distribution 2 Gyr ago, pre-LMC infall. Finally, we posit radial profiles of simulated MW-mass analogs also hosting an LMC companion are likely to evolve similarly to our results, such that the accretion of a massive satellite along with its satellites will lead to a more concentrated radial profile as the massive satellite advances toward its host galaxy.

Keywords: Dwarf galaxies (416) — Galaxy evolution (594) — Milky Way Galaxy (1054) — Large Magellanic Cloud (903)

1. INTRODUCTION

It is well known that dozens of known satellite galaxies and counting surround the Milky Way (MW) and Andromeda (M31). These satellites are largely low-mass dwarf galaxies often used to test cold dark matter theory with a cosmological constant (Λ CDM) on small scales. The abundance and spatial distribution of satellites can also illuminate the properties and underlying distribution of the dark matter halos surrounding the MW and M31.

In the era of high precision astrometry, observatories such as the *Hubble Space Telescope* and *Gaia* are pro-

viding precise proper motions for low mass dwarfs to the edge of the Local Group (LG; e.g., [van der Marel et al. 2012a](#); [Sohn et al. 2013, 2017, 2020](#); [Bennet et al. 2024](#)). These observatories will be complemented shortly by data from *JWST* and the *Nancy Grace Roman Space Telescope*, which will deliver additional precise proper motions for nearby galaxies.

Combined with line-of-sight (LOS) velocities and distances, proper motions yield 6-dimensional (6D) phase space information that can aid in reconstructing the recent accretion and evolutionary history of satellites in the LG. Indeed, the availability of this 6D data has already helped us make great strides in improving our knowledge of the Local Group’s dynamical history. Some examples include determining the orbit of the LMC around the MW ([Kallivayalil et al. 2013](#)), calculating the timing of the future MW-M31 encounter (e.g., [van der Marel et al. 2012, 2019](#)), constraining the orbit

Corresponding author: Ekta Patel
ekta.patel@utah.edu

* NASA Hubble Fellow

of M33 around M31 (e.g., [Patel et al. 2017](#)), studying the infall of satellites with the LMC (e.g. [Erkal & Belokurov 2020](#); [Patel et al. 2020](#); [Battaglia et al. 2022](#)), exploring the thin, planar structure of MW and M31 satellites (e.g. [Libeskind et al. 2005](#); [Pawlowski & Kroupa 2019](#); [Sohn et al. 2017, 2020](#)); and estimating the masses of the MW, M31, and the LG as a whole (e.g. [Patel et al. 2017b, 2018](#); [Patel & Mandel 2022](#); [Chamberlain et al. 2022](#); [Benisty et al. 2022](#); [Benisty 2024](#)).

Improved methods for modeling the orbits of satellite galaxies, especially the MW’s most massive satellite galaxy – the LMC – have proven to be especially useful. Using *HST* proper motions, [Kallivayalil et al. \(2013\)](#) showed the LMC is likely on first infall into the halo of the MW, having just completed a pericentric passage (see also [Besla et al. 2007](#)). It is also now known that the total mass of the LMC is likely $1 - 3 \times 10^{11} M_{\odot}$, or at least 10% the mass of the MW (e.g., [Shipp et al. 2021](#); [Watkins et al. 2024](#)).

With a precise mass and orbit for the LMC, several authors have made recent breakthroughs in understanding the impact of the LMC on the MW and corresponding substructures. These include quantifying the displacement and reflex motion of the MW’s center of mass, predicting the formation of a dark matter wake in the MW’s halo, and assessing biases in MW mass estimators resulting from the MW’s response to the gravitational influence of the LMC (e.g. [Garavito-Camargo et al. 2021](#); [Erkal & Belokurov 2020](#); [Lilleengen et al. 2023](#); [Vasiliev 2023](#); [Kravtsov & Winney 2024](#)). Both predictions and observations of these phenomena (e.g., [Erkal et al. 2021](#)) have collectively indicated the MW is not in equilibrium, contrary to previous assumptions.

Given this new knowledge, we must revisit traditional ways we have attempted to place the MW in the context of MW-mass galaxies at low redshift. Recently, both the Satellites Around Galactic Analogs (SAGA; [Mao et al. 2024](#)) survey and the Exploration of Local VolumE Satellites (ELVES; [Carlsten et al. 2022](#)) surveys have completed a census of satellite galaxies around MW-mass hosts down to $M_V = -11.9$ and $M_V = -9$, respectively ([Mao et al. 2024](#); [Carlsten et al. 2022](#)). Together, these surveys have taken a census of satellites around ~ 130 systems, providing a statistically significant sample for comparison with satellites of the MW.

Alongside these critical observational advances, studies using suites of cosmological zoom-in simulations of MW-mass halos have also proven exceptionally useful in placing the properties of MW satellites in context. We refer readers to [Samuel et al. \(e.g. 2020, 2021, 2022\)](#) and [Santistevan et al. \(2023, 2024\)](#) for analyses of the FIRE-2 cosmological zoom-in baryonic suite, Latte, centered

on MW-like galaxies, and the ELVIS on FIRE suite centered on LG-like pairs. For studies of subhalos around MW-mass halos in dark-matter-only suites of cosmological zoom-in simulations, we refer readers to [Kravtsov & Winney \(e.g., 2024\)](#) and [Buch et al. \(2024, hereafter B24\)](#) who study the Caterpillar simulations and Symphony/Milky Way-est dark matter only simulations, respectively.

Previously, studies comparing observed and simulated MW-mass galaxies typically focused on their present-day characteristics, neglecting historical evolution. With the advent of 6D phase space data and orbital modeling, we can conduct more comprehensive analyses of the MW’s properties across different epochs. This advancement enables us to assess how typical the MW is among similar-mass galaxies in both the local Universe and simulations and whether its current evolutionary stage is representative of MW-mass analogs. In light of recent findings on the significant impact of the LMC on the MW over the past ~ 2 Gyr, it is especially crucial to also account for its impact on the evolution of MW substructures.

In this paper, we quantify how the radial distribution of MW satellite galaxies changes as a function of time, including the influence of the LMC. This paper is organized as follows. In Section 2, we introduce the observational data used as input to the orbital models described in Section 3. Section 3 also details how radial profiles are generated as a function of time. In Section 4, we present our results for the total sample of MW satellites and when we exclude the impact of the LMC. Section 5 includes comparisons to surveys of MW-mass galaxies and the properties of simulated MW-mass analogs. Finally, we summarize and conclude in Section 6.

2. DATA

We use 6D phase space information derived from the combination of LOS velocity, distance modulus, and proper motions to integrate the orbital histories of MW satellite galaxies. From these orbital histories, we extract distances with respect to lookback time to construct radial profiles at present and past epochs.

Our primary observational data is from [McConnachie & Venn \(2020b\)](#), which used *Gaia* eDR3 to uniformly derive proper motions for 58 MW satellites. We also adopt the LOS velocities provided in [McConnachie & Venn \(2020b\)](#) and the R.A., Dec., and distance moduli provided in [McConnachie & Venn \(2020a\)](#). Absolute magnitude estimates are from [McConnachie \(2012\)](#) and [Simon \(2019\)](#).

Our sample of MW satellites includes the 45 galaxies reported in [McConnachie & Venn \(2020b\)](#) with a

measured LOS velocity and are within 300 kpc of the MW. The faintest dwarf in our sample is Draco II ($M_V = -0.8^{+0.4}_{-1.00}$; Simon 2019). We also include the LMC and SMC in our sample. When we evaluate the present-day distribution of satellite galaxies, we include the Sagittarius dwarf spheroidal (Sgr dSph) for consistency with other recent works. However, we exclude it when we evaluate the distribution of satellites at 1 and 2 Gyr ago as it has undergone significant disruption and mass loss by tides from the MW, which are not accounted for in our orbital models (e.g., Law et al. 2005).

Throughout this analysis, a distance (D) cut of 300 kpc ($D < 300$ kpc) is applied consistently at each epoch where we tabulate the MW’s cumulative radial profile. The total sample of satellites is $N_{\text{sat}} = 48$ at present-day, $N_{\text{sat}} = 47$ at 1 Gyr ago, and $N_{\text{sat}} = 45$ at 2 Gyr ago, on average, when distance uncertainties are included.

3. METHODS

Here, we describe the methods used to reconstruct orbital histories for each MW satellite and how orbital information is used to construct radial profiles for MW satellite galaxies.

3.1. Orbital Histories

We adopt and modify the methods from Patel et al. (2020, hereafter P20) to calculate the orbital histories of MW satellite galaxies through numerical integration backward in time in a joint MW+LMC gravitational potential. Orbits are initialized with the 6D phase space information (i.e., Galactocentric 3D position and 3D velocity) described in Section 2. We compute a direct orbital history (i.e., the orbit resulting directly from the transformation of measured quantities to 6D phase space vectors) for each satellite in our sample, where the given satellite, the MW, and the LMC are treated as a 3-body system.

As in other works (e.g., Patel et al. 2020; Richstein et al. 2022; Bennet et al. 2024), direct orbital histories represent one orbital solution per satellite galaxy. They do not account for the measurement uncertainties on LOS velocity, distance modulus, and proper motions. We return to these uncertainties at the end of this section.

Some important modifications to the P20 orbit methodology for this work include:

- The MW’s dark matter halo is modeled as a Hernquist sphere with a mass of $M_h = 1.57 \times 10^{12} M_\odot$ and scale length $a_{\text{halo}} = 40.85$ kpc. This M_h corresponds to a virial mass of $M_{\text{vir}} = 1.2 \times 10^{12} M_\odot$ and a virial radius of $R_{\text{vir}} = 279$ kpc.

- The MW’s disk is a Miyamoto-Nagai profile with a mass of $M_d = 5.78 \times 10^{10} M_\odot$ with disk scale length $r_a = 2.4$ kpc and disk scale height $r_b = 0.5$ kpc.
- The MW’s bulge is a Hernquist sphere with a mass of $M_b = 1.4 \times 10^{10} M_\odot$ and scale length $a_{\text{bulge}} = 0.7$ kpc. The MW’s disk, halo and bulge parameters are chosen to yield best-fit models to the observed rotation curve of the MW (McMillan 2017).
- The LMC is modeled as a one-component dark matter halo following a Hernquist profile (i.e., there is no stellar disk as in P20). The adopted virial mass is $M_{\text{vir}} = 1.8 \times 10^{11} M_\odot$ (the fiducial LMC mass in P20) with a Hernquist scale length $r_a = 20$ kpc. The scale length is determined by finding the best fit to the LMC’s measured rotation curve (van der Marel & Kallivayalil 2014).
- Dynamical friction owing to the MW and the LMC are both included; however, the dynamical friction satellites experience as they pass through the LMC’s halo is always in effect, whereas in P20 it was only implemented when a satellite was inside the outer equal density contour of the MW-LMC potential.

These modifications are adopted to reflect the initial conditions for the MW-LMC simulations presented in Garavito-Camargo et al. (2019)¹. In this setup, the LMC is on a first infall orbit where it starts at the MW’s virial radius ($R_{\text{vir}} = 279$ kpc) at 2.22 Gyr ago and arrives at its observed position today after passing through pericenter 60 Myr ago (see the orbit of LMC3 in Fig 2 of Garavito-Camargo et al. 2019).

As in P20, measurement errors on LOS velocity, distance, and proper motion for each satellite are accounted for by drawing 1,000 Monte Carlo samples from the joint 1σ uncertainties of these measured quantities. Each drawing is then converted to a 6D phase space vector in Galactocentric Cartesian coordinates and used to initialize a unique orbit per MW satellite. This process is repeated 1,000 times in the combined MW+LMC potential, yielding 1,000 possible orbital solutions for each MW satellite. In Section 3.2, we will use distances extracted from these orbits to build radial profiles as a function of time.

¹ The orbit methodology used here will be the basis for a forthcoming `Python` package that will allow users to integrate orbits of MW substructures in a joint MW+LMC potential both in rigid and live halos (Garavito-Camargo et al., in prep. & Patel et al., in prep.). Here, we adopt the rigid setup.

We ignore the 6D phase space uncertainties of the LMC as these are much smaller than those of the fainter satellite galaxies in our sample. The most significant uncertainties for satellite orbits are the choice of MW and LMC masses, followed by the uncertainties on proper motions and distances. For example, keeping the adopted mass of the LMC fixed and increasing the mass of the MW can allow for multiple passages of the LMC around the MW (e.g., [Patel et al. 2017, 2020](#)).

To isolate the LMC’s gravitational influence, we also consider a rigid potential with just the MW with parameters identical to those used in the combined MW+LMC potential. For the rigid MW potential, we also compute 1,000 orbits for each satellite galaxy as a control sample.

Our orbit methodology, which uses a multi-component potential with a rigid halo for the MW and a rigid, spherical halo for the LMC does not account for the halo deformations the MW experiences as the LMC passes through pericenter ([Garavito-Camargo et al. 2019](#)). It also does not track the tidal mass loss experienced by the LMC and the formation of the dark matter wake trailing the LMC ([Garavito-Camargo et al. 2019](#)). In future work, we will explicitly account for these halo perturbations using gravitational potentials that capture the full time-evolution of the MW+LMC interaction simulated in [Garavito-Camargo et al. \(2019\)](#) by employing basis function expansions ([Garavito-Camargo et al. 2021](#)) to reconstruct the joint MW+LMC potential.

3.2. Constructing Cumulative Radial Profiles

Our goal is to explore the evolution of the radial distribution of MW satellites over the last ~ 2 Gyr, equivalent to the time it takes the LMC to move from the edge of the MW’s halo to its present-day position in a first infall scenario. At each time step (0, 1, 2 Gyr ago), we calculate the cumulative radial profile (also referred to as radial profile throughout) for the set of satellites within 300 kpc of the MW. The cumulative radial profile sums up the number of satellite galaxies within a given distance. We build 1,000 radial profiles for each time step by extracting distances from the 1,000 orbital histories computed for each satellite galaxy (see Section 3.1).

The top left panel of Figure 1 shows the resulting radial profiles at present-day (solid blue line), 1 Gyr ago (dashed orange line), and 2 Gyr ago (dotted green line). The lines represent the medians, or 50th percentiles, of the 1,000 radial profiles generated for each time step. The shaded regions in the top panel of Figure 1 encompass the [15.9, 84.1] percentiles (68%) around the median radial profile.

As distance uncertainties grow proportionally with the timescale of orbital integration, the extent of the shaded

region at 2 Gyr ago is the largest, followed by the radial profile at 1 Gyr ago sample, with the present-day radial profile having the smallest uncertainty. In other words, the present-day distance uncertainties are equivalent to the measurement error on the distance modulus for each satellite, while the distance uncertainty at 1 Gyr ago and 2 Gyr ago simultaneously account for the propagation of all uncertainties on LOS velocity, distance, and proper motion.

4. RESULTS

In this section, we quantify the properties of radial profiles as a function of time and determine what drives the evolution between different epochs. We also examine the influence of the LMC on the orbits of MW satellites and, subsequently, on the radial distribution of the satellite population.

4.1. Properties of Radial Profiles in the MW+LMC Potential

The top left panel of Figure 1 illustrates the radial profiles for all satellites within 300 kpc of the Galaxy’s center at present-day, 1 Gyr ago, and 2 Gyr ago, respectively. The total number of satellites included in the median radial profile at each time is 48 (present-day), 47 (1 Gyr ago), and 45 (2 Gyr ago). To quantify the concentration of the radial profiles at each time, we use the R_{50} statistic, the radius encompassing half of the total satellite population. Since the number of satellites included in the present-day, 1 Gyr ago, and 2 Gyr ago samples is not identical, R_{50} is calculated self-consistently with respect to each sample’s size. We find the following values for R_{50} : 71 kpc (present-day), 102 kpc (1 Gyr ago), and 112 kpc (2 Gyr ago), as denoted by the vertical lines in the top panel of Figure 1. The present-day location of the LMC is marked with a black dot dashed line.

The present-day radial profile (blue line) is most highly concentrated compared to the radial profiles at previous epochs. While $R_{50}=71$ kpc implies 50% of satellites reside within $D < 71$ kpc, nearly 80% of the total population is located within 150 kpc. On the other hand, the radial profiles at 1 and 2 Gyr ago have shallower slopes within 150 kpc, implying MW satellites were more spatially dispersed in the past. Direct orbital histories from Section 3.1 also show that $\sim 40\%$ of satellite galaxies are moving toward the MW approaching present-day on first infall orbits, driving the decreasing R_{50} values (and slopes) approaching present-day. Beyond 150 kpc, the radial profiles at present-day and 1 Gyr ago are qualitatively consistent, differing by just one additional satellite in the present-day sample. In comparison, the radial profile at 2 Gyr ago grows more gradually at $D > 150$ kpc.

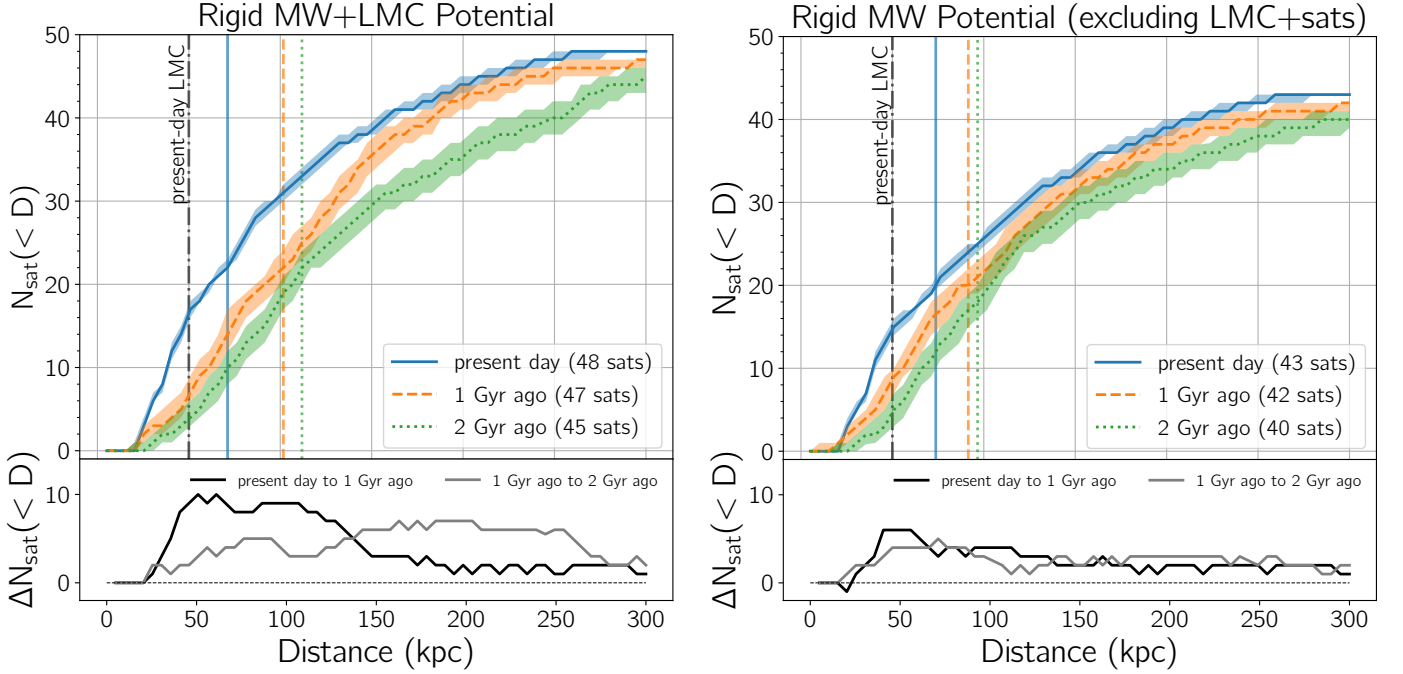


Figure 1. Left: (Top) The cumulative number of satellite galaxies as a function of 3D distance relative to the MW at present-day (solid blue), 1 Gyr ago (dashed orange), and 2 Gyr ago (dotted green) from orbits calculated in a joint MW+LMC potential. Shaded regions correspond to the 68 percent confidence intervals on the radial distribution at each time. Colored vertical lines illustrate the R_{50} value for each data set, the radius at which half of the satellites are encompassed. The black vertical line shows the present-day location of the LMC. The legend indicates how many satellites are included at each time step. We do not correct for completeness. (Bottom) The difference between pairs of radial distributions as a function of 3D distance. The black line shows the difference between the present-day and 1 Gyr ago radial profiles, while the gray line indicates the difference between the 1 and 2 Gyr ago distributions. Radial profiles are less concentrated at previous epochs compared to today. The largest differences in radial profiles between present-day and 1 Gyr ago are in the innermost regions ($D < 150$ kpc), while the difference between the radial profile at 1 and 2 Gyr ago is more apparent in the outer regions ($D > 150$ kpc). **Right:** (Top) Same as left panel, but the gravitational influence of the LMC has been removed, as well as the LMC plus four satellites within R_{vir} of the LMC at infall (2.2 Gyr ago) and today. These satellites include the SMC, Carina III, Phoenix II, and Sculptor. (Bottom) The difference between radial distributions for present-day and 1 Gyr ago (black) and 1 Gyr ago to 2 Gyr ago (gray). The radial distributions evolve minimally compared to Figure 1, implying that the presence of the LMC and its satellites drive the redistribution of satellites over time.

The orbits of MW satellites in the rigid MW+LMC potential also respond to the reflex motion and displacement of the MW’s center of mass as the LMC passes through the MW’s halo. This phenomenon shifts the MW’s center of mass by up to 40 kpc over the last 2 Gyr, with 80% of this effect taking place in just the previous Gyr (Garavito-Camargo et al. 2021). The impact of the LMC on the MW likely explains the significant evolution of the radial profile, particularly between 1 Gyr ago and today.

Furthermore, Kravtsov & Winney (2024) recently analyzed the highest resolution, dark-matter-only simulations in the Caterpillar suite, which zooms in on MW-mass halos (Griffen et al. 2016), to investigate the impact of an LMC-mass analog on the distance and ve-

locity distribution of MW satellites². These authors use two specific halos from the Caterpillar suite hosting a massive satellite like the LMC that recently ($z \approx 0.04 - 0.05$) passed through a close, pericentric passage ($r_{\text{peri}} = 40 - 50$ kpc). In Figure 6, they show the radial distribution of satellite positions becomes more concentrated at pericenter and corresponds to a high-velocity tail in the cumulative 3D velocity distribution of MW satellites owing to the response of the MW analog to the LMC analog’s passage.

In our analysis, the LMC passes through pericenter at ~ 60 Myr, approximately corresponding to our present-

² Kravtsov & Winney (2024) also use their results to develop a new mass estimator correcting for the impact of the LMC on satellite kinematics, finding $M_{200c} = 9.96 \pm 1.45 \times 10^{11} M_{\odot}$. Our assumed MW mass for satellite orbits (see Section 3.1) is consistent within the scatter of the Kravtsov & Winney (2024) mass results.

day results in Figure 1, where we also see the highest concentration in the radial distance distribution. This agrees with the results of Kravtsov & Winney (2024). In Section 4.2, we will further examine the influence of the LMC on the distribution of MW satellites.

The bottom left panel of Figure 1 shows the difference between the cumulative radial profiles at each pair of time steps. We denote this difference (also referred to as a differential radial profile throughout) as $\Delta N_{\text{sat}}(< D)$, the difference in the cumulative number of satellites present within a specific distance at two different times. The black line represents the radial profile at 1 Gyr ago subtracted from the present-day radial profile, while the gray line shows the radial profile at 2 Gyr ago subtracted from the radial profile at 1 Gyr ago. Whether $\Delta N_{\text{sat}}(< D)$ increases or decreases describes how satellites are redistributed across the MW’s halo over time. By this definition, $\Delta N_{\text{sat}}(< D) > 0$ corresponds to a net increase in the cumulative number of satellites between time steps, while $\Delta N_{\text{sat}}(< D) < 0$ corresponds to a net decrease in the cumulative number of satellites.

In the bottom left panel of Figure 1, the most significant periods of evolution in the radial profiles between present-day and 1 Gyr ago (black line) occur between ~ 25 –150 kpc. Beyond 150 kpc, this differential is approximately constant, indicating little to no net change in the number of satellites at these distances. This does not imply that satellites are not moving to different radial distances; rather, the net change in the number of satellites changes minimally as a function of distance. The differential quantifying the change in radial profiles at 1 Gyr ago and 2 Gyr ago (gray line) shows consistent but more gradual differences across the full range of distances.

In Appendix A, we examine the distances and orbits of satellite galaxies to determine which specific satellites drive the evolution of radial profiles from one time step to the next.

4.2. Removing the Influence of the LMC and its Satellites

Several recent works have reported which of the ultra-faint dwarf galaxies discovered in the vicinity of the LMC/SMC are potential satellites of the LMC having entered the halo of the MW as a group (e.g., Jethwa et al. 2016; Sales et al. 2017; Erkal & Belokurov 2020; Patel et al. 2020). Independent methodologies based on both position and phase space arguments have been applied to conclude which satellites belong to the LMC (see Vasiliev 2023, for a review). Typically, the SMC is implicitly accounted for in a first infall scenario.

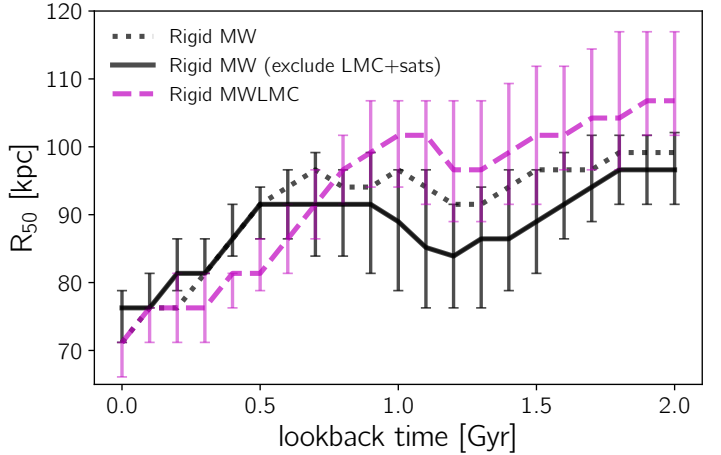


Figure 2. The evolution of R_{50} with time for all satellites in the Rigid MW+LMC potential (dashed magenta line), all satellites in the Rigid MW potential (dotted black line), and satellites in the Rigid MW potential excluding the LMC and its satellites (solid black line). Lines track the median of R_{50} across 1,000 radial profiles constructed at each time step. Error bars represent the 25th and 75th percentiles of R_{50} .

For this analysis, we aim to isolate the influence of the LMC itself and the group of satellites that may have entered the MW’s halo alongside it. We identify LMC satellites as those within R_{vir} of the LMC (148 kpc) and 300 kpc of the MW at infall (2.2 Gyr ago) as in Nadler et al. (2020). These satellites include the SMC, Carina III, Phoenix II, and Sculptor. We will revisit which MW satellites evidence a shared orbital history with the LMC using the metrics developed in P20 in forthcoming work that will explore the effects of the time-evolving joint MW+LMC potential on MW satellites (Garavito-Camargo et al., in prep.; Patel et al., in prep.).

We repeat the exercise of building MW radial profiles by i.) excluding the LMC’s gravitational influence (i.e., using orbits computed in a rigid MW-only potential) and ii.) removing the SMC, Carina III, Phoenix II, and Sculptor from the satellite sample at all time steps. The top right panel of Figure 1 presents the resulting radial profiles. The total number of satellites in each sample is as follows: 43 (present-day), 42 (1 Gyr ago), and 40 (2 Gyr ago). The corresponding R_{50} values are 74 kpc (present-day), 92 kpc (1 Gyr ago), and 97 kpc (2 Gyr ago).

Compared to the results presented for the rigid MW+LMC radial profiles in Section 4.1 (top left panel of Figure 1), the top right panel of Figure 1 qualitatively shows less evolution. This is quantitatively captured by the R_{50} markers in the top right panel of Figure 1, which have a significantly narrower range, approximately half the span of the R_{50} values presented in the top left panel

of Figure 1. The bottom right panel of Figure 1 shows the difference in pairs of radial profiles, which remain approximately constant at $D > 75$ kpc. Appendix A further explores the redistribution of satellites with time.

To determine the magnitude of the LMC’s gravitational influence, we calculate R_{50} as a function of time for *all satellites* within 300 kpc of the MW in the rigid MW-only potential compared to the MW+LMC potential. The results are presented in Figure 2, where the black dotted line corresponds to the rigid MW results, and the dashed magenta line corresponds to the rigid MW+LMC results. While both lines intersect at present, R_{50} varies across a larger range (~ 70 -105 kpc vs. ~ 70 -95 kpc) when the influence of the LMC is captured. Figure 2 also shows the results for the Rigid MW potential when the LMC and its satellites are removed (solid black line), as in the top right panel of Figure 1. The range of R_{50} narrows for the rigid MW potential when these five satellites are excluded. Figure 1 concisely illustrates the individual effects of the LMC and its satellites on the concentration of radial profiles, with the impact of the LMC being slightly more than that of its satellites.

We conclude the LMC’s gravitational influence and group infall play key roles in the evolution of the MW’s radial profile. Additionally, we have only considered an LMC mass of $1.8 \times 10^{11} M_{\odot}$, but current upper limits for the mass of the LMC reach $\sim 3.5 \times 10^{11} M_{\odot}$ (see Watkins et al. 2024, for a compilation). P20 and Garavito-Camargo et al. (2021) have shown the impact of the LMC on satellite orbits, and the MW increases proportionally with mass; therefore, the results presented here are expected to scale up in the case of a more massive LMC. In the absence of a massive satellite galaxy on recent infall, we expect minimal evolution in radial profiles as a function of time. We caution studies aiming to compare the radial profile of the actual MW with MW analogs in both simulations and observations to proceed with this in mind.

There are other effects to note that also contribute to the evolution of the MW’s radial profile, though to a lesser degree. These effects include the changing orbital configuration of satellites (i.e., whether satellites are at pericenter, apocenter, or somewhere in between at the three epochs of interest) and satellite distance uncertainties. When distance uncertainties are ignored, radial profiles are not equivalent to those shown in Figure 1. This reflects that direct orbits differ from the median of 1,000 orbital solutions computed per satellite and that distance uncertainties can give rise to some evolution in the radial profiles. Finally, we remind readers that the census of MW satellites is not yet complete

and specifically that a majority of MW satellites are currently closer to pericenter than apocenter (see Fritz et al. 2018). This implies many more distant MW dwarfs are yet to be discovered. If satellites exist at larger distances, the present-day radial profiles may not exhibit such high concentrations; however, it is unclear exactly how radial profiles would evolve backward in time with a complete census of MW satellites.

5. DISCUSSION

Here, we compare the results reported in Section 4 to observations of MW-like galaxies in the local Universe and simulated MW analog galaxies. We aim to determine whether the present-day MW is more representative of its galactic counterparts, or if the MW was more representative of other MW-like galaxies at earlier epochs in its evolution.

5.1. Comparisons to Observational Analogs of the Milky Way

Many recent efforts have been made to characterize satellite populations around MW/M31-mass galaxies beyond the Local Group (e.g., Spencer et al. 2014; Danieli et al. 2017; Smercina et al. 2018; Kondapally et al. 2018; Bennet et al. 2019; Crnojević et al. 2019; Bennet et al. 2020). A diverse range of host galaxy systems have been studied to different limiting magnitudes, revealing that they exhibit a wide variety in the number of satellite galaxies they harbor and in the properties of those satellite galaxies.

We focus specifically on the results of the SAGA survey (Geha et al. 2017; Mao et al. 2021, 2024) and the ELVES survey (Carlsten et al. 2022). The latest SAGA data release (Data Release 3, DR3) contains 101 systems at 25-40 Mpc, with satellites down to $M_V = -11.9$ mag. ELVES includes 28 systems within 12 Mpc, reaching satellites down to $M_V = -9$ mag. In what follows, we will compare the average radial profiles of host systems in these surveys to our results using the R_{50} statistic. We will leave a more in-depth analysis linking the properties of satellites (i.e., color, stellar mass, quenching time) and their evolving radial distances to future work.

As the SAGA survey is only complete to a limiting magnitude of $M_{r,0} < -12.3$ mag (or $M_V < -11.9$ mag), in this exercise, we consider only the MW satellites passing this magnitude selection³. This consists of the LMC, SMC, Sgr, Fornax, and Leo I. Using the distances ex-

³ The ELVES survey is complete down to $M_V \sim -9$ mag, but we only include satellites down to $M_V = -11.9$ for consistent comparisons between SAGA, ELVES, and our results.

$$M_V < -11.9 \text{ mag}; D < 300 \text{ kpc}$$

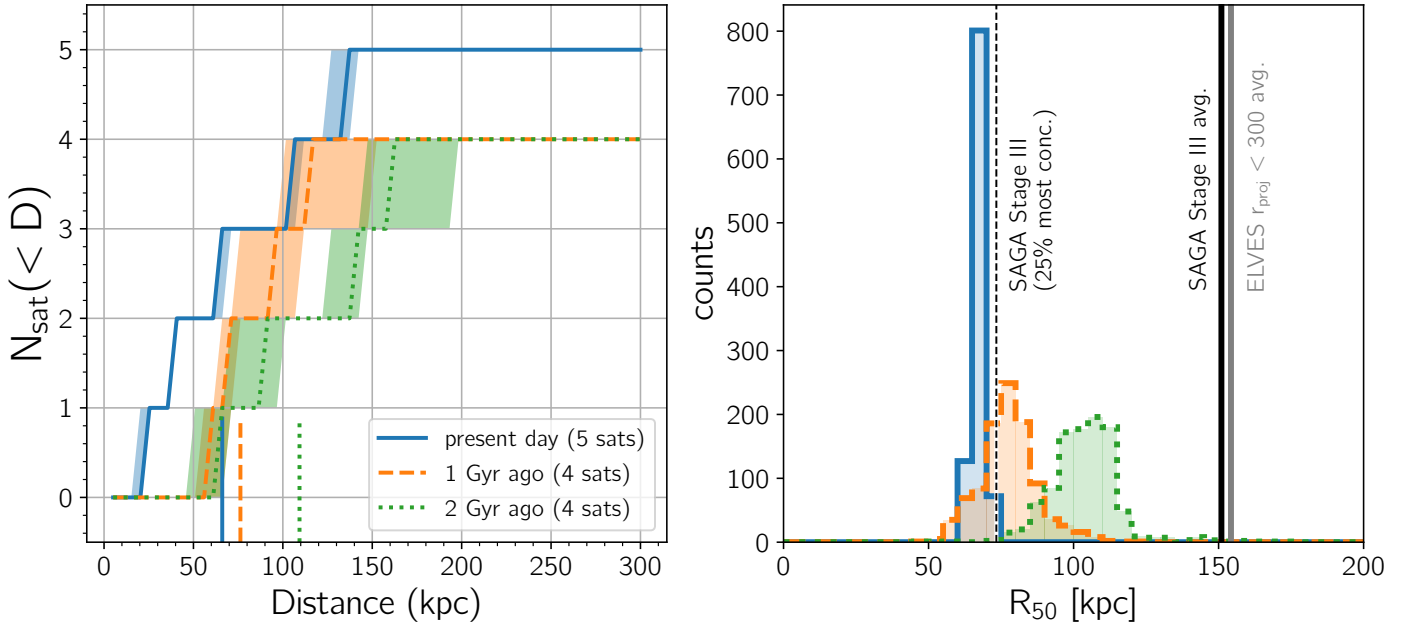


Figure 3. Left: The cumulative radial profile for satellites with $M_V < -11.9$ mag at $D < 300$ kpc in the joint MW+LMC potential. This magnitude selection reduces the MW sample to only four or five satellites, as indicated in the legend. **Right:** The distribution of R_{50} , the radius encompassing half of the satellites within 300 kpc of the MW, at present-day (blue histogram), 1 Gyr ago (orange histogram), and 2 Gyr ago (green histogram) for satellites with $M_V < -11.9$ mag. The thick black line represents the average R_{50} for the 101 hosts included in Data Release 3 (DR3) of the SAGA survey (Mao et al. 2024). The thin, dashed black line represents R_{50} for the subset of the 25% most concentrated SAGA DR3 hosts. The thick gray line illustrates the average R_{50} from a sample of hosts included in the ELVES survey (Carlsten et al. 2022). The MW’s present-day R_{50} is most consistent with the highly concentrated hosts in SAGA DR3, while the average SAGA DR3 and ELVES R_{50} values are significantly larger than the MW population even at 1-2 Gyr ago.

tracted from the 1,000 orbital histories computed for each satellite in Section 3.1, we compute 1,000 radial profiles at each time step for this subsample. The resulting median radial profiles and 68% confidence intervals are presented in the left panel of Figure 3. As in Section 4, we consistently apply a distance cut of 300 kpc. Even with a small sample of only the brightest satellites, the evolution of the radial profile is still evident.

The right panel of Figure 3 shows the distribution of R_{50} for the present-day (blue), 1 Gyr ago (orange), and 2 Gyr ago (green) radial profiles. Each histogram represents 1,000 R_{50} values corresponding to 1,000 radial profiles. The two black vertical lines correspond to R_{50} for SAGA DR3, where the thick black line represents the average of all 101 systems and the thin, dashed black line is the average of the 25% most concentrated systems from Mao et al. (2024).

The gray line corresponds to the average R_{50} from the ELVES survey (Carlsten et al. 2022). For ELVES, R_{50} is computed for only those satellites with $M_V < -12$ mag in the ten hosts passing the SAGA host selection criteria and have coverage to 300 kpc. These ten hosts include NGC 253 (2 satellites), 628 (11), 1291 (9), 2683

(2), 2903 (4), 3115 (7), 4736 (1), 5055 (6), 5236 (7), and 5457 (5), where the numbers in parentheses indicate the number of satellites with $M_V < -12$ mag.

Generally, our R_{50} values are significantly smaller at all epochs compared to the SAGA DR3 and ELVES R_{50} lines at ~ 150 kpc. The latter minimally intersects with the high tail end of our R_{50} histogram at 2 Gyr ago (green histogram). On the other hand, the most highly concentrated SAGA systems are approximately consistent with our present-day MW results (blue histogram), however, the most concentrated systems in SAGA are not strictly those that host LMC-mass analogs. We conclude that MW is amongst the most radially concentrated satellite systems across observed MW analogs, even at 2 Gyr ago.

5.2. Comparisons to Simulated Analogs of the Milky Way

Multiple recent studies have characterized the radial profile of MW analogs in both isolated and Local Group-like (LG-like) environments using cosmological zoom-in simulations. We use these studies to place our results in the context of statistically significant samples of MW

analogs with a broad range of formation and evolutionary histories.

5.2.1. Latte and ELVIS on FIRE Simulations

Samuel et al. (2020, hereafter S20) analyzed the radial profile of simulated MW analogs in both isolated and LG-like (i.e., with an M31-mass companion) environments. Two suites of cosmological zoom-in baryonic simulations were used, namely the Latte suite of ten halos with $M_{200m} = 0.9 - 2 \times 10^{12} M_{\odot}$ and the ELVIS on FIRE suite (Garrison-Kimmel et al. 2019) which includes two pairs of MW-M31 analogs (i.e., Local Group-like pairs, also denoted as LG-like pairs). All satellites with stellar masses $M_* > 10^5 M_{\odot}$ and distances within 300 kpc of their host halos were considered. Results were averaged over simulation snapshots corresponding to the last ~ 1.3 Gyr.

S20 conclude the radial profiles of their isolated MW analogs from Latte at $z \approx 0$ are broadly consistent with observations of the MW and M31 within 150 kpc. However, they predict the MW may have 2-10 galaxies with $M_* > 10^5 M_{\odot}$ that have yet to be discovered. Searches of the Sloan Digital Sky Survey, on the other hand, claim the MW’s satellite population is complete down to $M_V = -6.5$ mag (Simon 2019, and references therein). Therefore, we directly compare our results to the simulation results without an additional completeness correction.

For consistency with S20, we select all MW satellites within 300 kpc with $M_V < -7.5$ mag (equivalent to $M_* > 10^5 M_{\odot}$). This magnitude selection limits the MW satellite sample to between 13 and 15 satellites, while the Latte suite has 17 satellites within 300 kpc, on average. The left panel of Figure 4 shows the resulting radial profiles at each time step. Again, we see evolution in the radial profiles, as shown in Section 4.

The middle panel of Figure 4 shows the distribution of R_{50} for the sample of satellites with $M_V < -7.5$. The results of all hosts in S20 are illustrated with a black vertical line. Compared to our distributions of R_{50} , all hosts from S20 typically have larger R_{50} values, which may be in part due to the prediction of several undiscovered satellites in the outskirts of the MW ($D > 150$ kpc). However, there is a narrow area of parameter space where the distribution of our results for MW satellites 2 Gyr ago (green histogram) intersects with the S20 results from the Latte suite. If we limit our satellite selection criteria only to include those within 150 kpc of the MW where S20 claim the MW population is complete, the simulated results (also limited to 150 kpc) intersect with the peak of the MW results at 2 Gyr ago,

and the upper end of the MW results at 1 Gyr ago, as illustrated in the right panel of Figure 4.

While the Latte sample of S20 does include two host halos with an LMC-mass analog, these analogs have orbits different from the LMC orbit adopted in this work (i.e., none of them pass through pericenter during the last 1.3 Gyr, the period over which their results are averaged). Therefore, it is not straightforward to evaluate how the influence of massive satellites like the LMC might affect the results of the simulated MW analogs in Latte, on average, compared to the actual MW-LMC system. Nevertheless, we conclude that the MW was more representative of MW analogs in simulations in the past than it is now.

5.2.2. Milky Way-est and Symphony Simulations

More recently, B24 characterized the properties of subhalos around 33 MW analogs in the “Milky Way-est” dark-matter-only (DMO), cosmological, zoom-in simulations. These halos are specifically chosen to host LMC analogs (based on its mass ratio to the MW and its orbit) and the ancient Gaia-Sausage-Enceladus merger (Helmi et al. 2018; Belokurov et al. 2018). B24 also study the properties of 45 isolated MW halos from the Symphony Milky Way suite as a control sample (Mao et al. 2015; Nadler et al. 2023). Since the MW satellite sample used in this analysis is not complete to the equivalent magnitude of the MW-est resolution limits⁴, we refrain from a quantitative comparison with B24 and instead focus on general trends between our results.

B24 find MW-est halos have $\approx 22\%$ more subhalos than the Symphony hosts due to the presence of an LMC analog and its associated subhalos, identified as those subhalos within R_{vir} of the corresponding LMC analog. They find half (11%) of these satellites are within R_{vir} of the LMC while the other half are within $2R_{\text{vir}}$ at the time when this region is entirely outside of the MW analog’s halo. Returning to our results from Section 4, we find 4/45 (9%) satellites are within R_{vir} of the LMC at infall (~ 2 Gyr ago). This validates our conclusion that the group infall of LMC satellites is one of the main drivers of our evolving radial profiles. However, DMO simulations, such as MW-est, do not account for the enhanced disruption of subhalos known to occur when a gravitational disk component is included (e.g., Garrison-Kimmel et al. 2017; Kelley et al. 2019; Wang et al. 2024). This effect is expected to reduce the number of subha-

⁴ The dark matter particle mass in the highest resolution regions of MW-est have a mass $m_{dm} = 4 \times 10^5 M_{\odot}$. B24 consider subhalos with present-day virial masses $M_{sub} > 1.2 \times 10^8 M_{\odot}$.

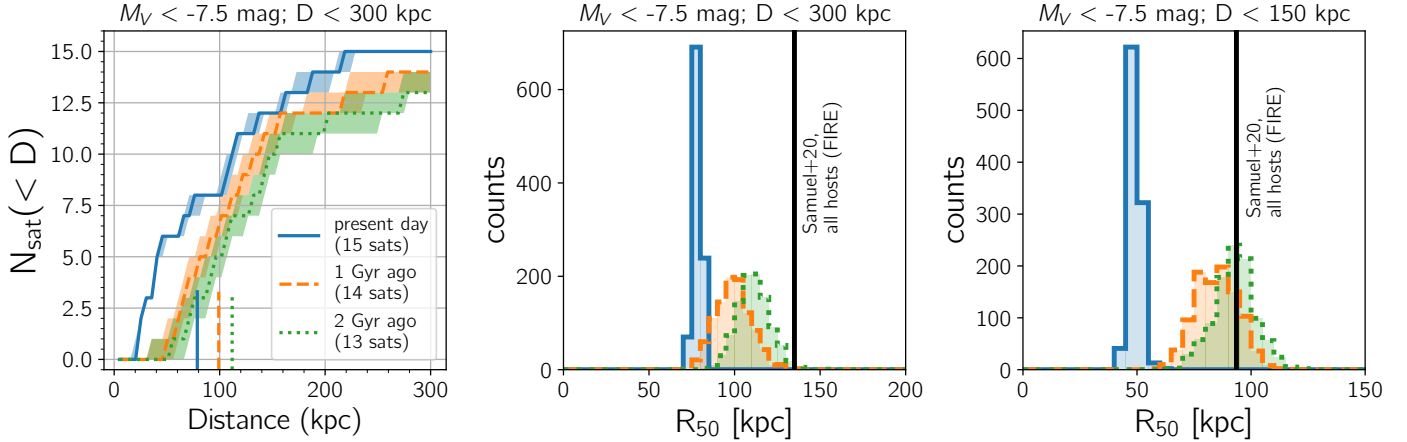


Figure 4. **Left:** Same as Figure 3 including all satellites with $M_V < -7.5$ mag, the magnitude equivalent to the resolution of the Latte simulations. This magnitude selection limits the MW satellite sample to 13-15 satellites, as indicated by the parenthetical in the legend. **Middle:** Same as Figure 3 for all satellites with $M_V < -7.5$ mag. The thick black line represents the average R_{50} for all Latte MW analogs analyzed in S20. Our results exhibit R_{50} values below those of Latte MW analogs, with only minimal overlap between our 2 Gyr ago results. **Right:** Same as the middle panel but only including satellites within 150 kpc. The black vertical line represents the average R_{50} for all Latte MW analogs analyzed in S20, also within 150 kpc. Our results for the MW at previous epochs are in good agreement with those from Latte, suggesting the MW may have been more representative of simulated analogs in past evolutionary phases.

los that survive to present-day, and therefore the B24 estimates should be considered an upper limit.

Based on the results presented in Figure 1, we predict the radial profiles of the isolated MW Symphony sample used in B24 are likely to remain approximately the same if they are traced back to 2 Gyr ago in the simulation, whereas the average radial profile of the MW-est host sample is likely to evolve similarly to our Figure 1 due to the infall of the LMC analogs and their associated satellites. This is beyond the scope of this analysis but will be the subject of future work.

6. SUMMARY AND CONCLUSIONS

We have quantified the MW’s cumulative radial profile evolution using all known MW satellites with measured 6D phase space within 300 kpc. We traced this evolution over the last 2 Gyr, corresponding to the LMC’s infall time (and its associated satellites). For comparison, we constructed radial profiles in both a joint MW+LMC potential and a rigid MW-only potential. Finally, we compared our results to observational surveys of MW-mass galaxies and cosmological zoom-in simulations of MW-mass analogs. Our main findings include:

1. We find the cumulative radial profile of MW satellites becomes more concentrated over the last 2 Gyr in a combined MW+LMC potential (left panels, Fig. 1), as exhibited by decreasing R_{50} values with time: 112 kpc (2 Gyr ago), 102 kpc (1 Gyr ago), and 71 kpc (present-day).

2. When we repeat our analysis in a MW-only potential removing the LMC and its four satellites (SMC, Carina III, Phoenix II, Sculptor), the evolution of the MW’s radial profile is weaker (right panels, Fig. 1). The R_{50} values for radial profiles excluding LMC satellites are 74 kpc, 92 kpc, and 97 kpc. This range is only half that of the R_{50} values for radial profiles computed in the MW+LMC potential.
3. We attribute the increased concentration over time to the LMC’s gravitational influence and the group infall of satellite galaxies associated with the LMC, though other less significant effects should also be considered. Our conclusions agree with recent work examining the radial profiles of simulated MW-mass analogs with and without an analog of the LMC’s mass and orbit (see Section 5.2).
4. We use a subset of our satellite sample (selected based on M_V) to compute and compare our radial profile results to those presented in the SAGA and ELVES surveys (Fig. 3). We conclude the MW’s current evolutionary state is rare amongst MW-mass systems in the local Universe. Instead, the MW’s present-day radial profile is most well-aligned with the 25% most concentrated SAGA systems.
5. Using a subset of galaxies (selected based on simulation resolution limits), we compute and compare our radial profiles to those of MW-mass analogs in

cosmological zoom-in simulations (Fig. 4). Considering satellites within 300 kpc of the MW, our results show the MW is not representative of simulated MW analogs at present-day, 1 Gyr ago, or 2 Gyr ago. When we limit the sample to only those satellites within 150 kpc, we find good agreement between the simulated analogs and our results for the MW at 1 and 2 Gyr ago, implying the MW was more similar to simulated counterparts in its previous evolutionary phases.

6. Based on our conclusions, we posit radial profiles of MW+LMC analogs (where analogous systems align with the estimated mass and orbit of the LMC) in simulations are expected to evolve to a greater degree compared to MW-like systems without a massive satellite companion.

In forthcoming work, we will quantify the gravitational influence of the LMC and its impact on the orbits of satellite galaxies using a joint MW+LMC potential (derived from the simulations of Garavito-Camargo et al. 2019) accounting for the evolution of the MW and the LMC’s dark matter halos over the last ~ 2 Gyr (Patel et al., in prep.). We will re-examine whether the LMC satellites previously concluded to be associated (e.g., P20) holds and how this might impact the evolution of the MW’s radial profile presented in this work. Furthermore, we will account for the impact of M31’s gravitational influence to determine if it has any effect on the distribution of MW satellites.

It is worth noting that the observational completeness of known MW satellite population is not homogeneous, as these dwarfs were discovered using instruments with varying sensitivity, and the sensitivity also depends on angular position. This poses an interesting question of whether the radial distribution evolves differently when these selection effects are taken into account. This will be explored in future work, but our current analysis with a more observationally complete sample (bright satellites within 150 kpc; as shown in the rightmost panel of Figure 4) suggests that the radial distribution still evolves inward with time.

As more Milky Way (MW) satellite galaxies are discovered, and their complete 6D phase space information is measured, it is crucial we continue to revisit our un-

derstanding of the distribution of these satellites around the MW. More than a dozen known satellites lack LOS velocities and/or proper motion data, which will significantly expand the viable sample of MW satellites once these measurements become available. These satellites are distributed across the MW’s halo from 25-250 kpc. Thus, they are unlikely to change the results presented here.

However, we have not yet considered the disrupted dwarf galaxies observed as stellar streams today. These dwarf progenitors would have been considered satellites in the past, depending on their disruption timescales. Since stellar streams tend to be within 50 kpc of the MW, including these dwarf progenitors in our radial profile analysis would likely skew the radial profiles toward lower R_{50} values compared to those in this work.

When sufficient phase space information becomes available for the satellite galaxies around Andromeda (M31), we can similarly examine how its radial profile evolves. This may reveal valuable clues about M31’s recent accretion history, potentially providing new insights into the formation and evolution of massive galaxy halos.

EP is supported by NASA through Hubble Fellowship grant # HST-HF2-51540.001-A, awarded by the Space Telescope Science Institute (STScI). STScI is operated by the Association of Universities for Research in Astronomy, Incorporated, under NASA contract NAS5-26555. EP thanks Dan Weisz for helpful discussions that contributed to the genesis of this project and Emily Strickland for providing early data files used to develop the comparison to the SAGA survey. The authors also thank Paul Bennet, Jenna Samuel, and Ethan Nadler for feedback that helped improve the quality of this manuscript. EP and LC express their gratitude to the organizers of the January 2023 Conference for Undergraduate Women in Physics at Texas Christian University. It was through this event that they were introduced to each other.

Software: Numpy (Harris et al. 2020), SciPy (Virtanen et al. 2020), Matplotlib (Hunter 2007), IPython (Perez & Granger 2007), Jupyter (Kluyver et al. 2016), Astropy (Astropy Collaboration et al. 2013; Price-Whelan et al. 2018; Astropy Collaboration et al. 2022), Gala (Price-Whelan 2017)

APPENDIX

A. THE RADIAL REDISTRIBUTION OF MW SATELLITES

The bottom left panel of Figure 1 shows significant changes in the differential radial profiles, $\Delta N_{\text{sat}}(< D)$,

between 1 Gyr ago and present-day, specifically at $D \sim 25 - 150$ kpc. Using satellite distances extracted from

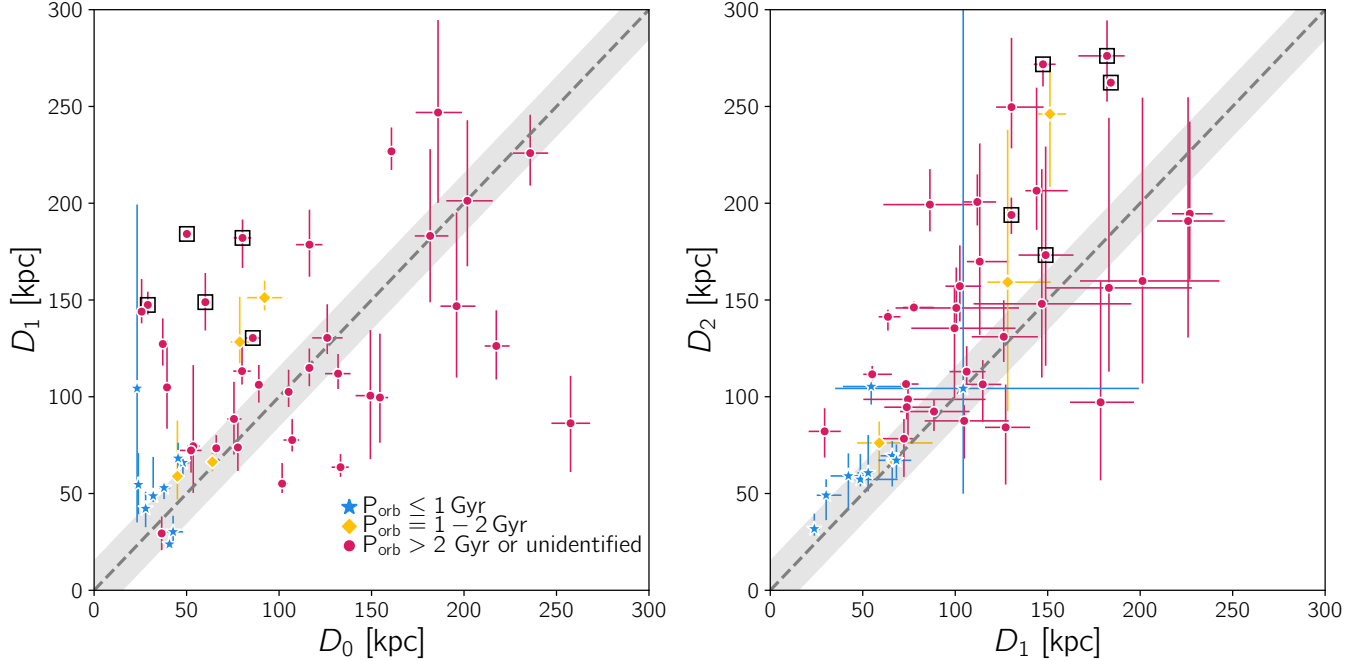


Figure 5. Left: The median distances of all galaxies within 300 kpc of the MW at present-day (D_0) and 1 Gyr ago (D_1). Error bars illustrate the extents of the 25th and 75th percentiles of distance from the 1,000 orbits using the Rigid MW+LMC potential described in Section 3.1. Blue stars represent satellites with short orbital periods ($P_{\text{orb}} \leq 1$ Gyr), yellow diamonds represent satellites with intermediate orbital periods ($P_{\text{orb}} = 1 - 2$ Gyr), and pink circles represent satellites with long ($P_{\text{orb}} > 2$ Gyr) or unidentified orbital periods. The gray dashed line represents a one-to-one correlation, and the corresponding shaded region encompasses ± 15 kpc. Open black squares denote the LMC and the four satellites identified as LMC satellites in Section 4.2. **Right:** Same as the left panel but at 1 Gyr ago (D_1) and 2 Gyr ago (D_2).

1,000 orbital histories computed in the rigid MW+LMC potential, determine how satellites are redistributed by visualizing distances compared to the length of each satellite’s orbital period.

The left panel of Figure 5 shows the median distance of all satellites at present-day (D_0) compared to their distances at 1 Gyr ago (D_1). Points are colored by the length of the orbital period (P_{orb}) such that blue stars are satellites with $P_{\text{orb}} \leq 1$ Gyr, yellow diamonds have $P_{\text{orb}} = 1 - 2$ Gyr and pink circles have either $P_{\text{orb}} > 2$ Gyr or an orbital period that cannot be determined during the 2 Gyr integration period. The gray dashed line represents a one-to-one correlation, and the corresponding shaded region encompasses ± 15 kpc. Black squares encompass the LMC and its four associated satellites.

Comparing D_1 and D_0 , 30% of satellites fall in the gray-shaded region, where distances have not changed by more than ± 15 kpc. In the distance range of interest, $D \sim 25 - 150$, most satellites with short orbital periods (blue stars) remain within $D \lesssim 50$ kpc at both epochs. Satellites with intermediate-length orbital periods (1-2 Gyr) stay at about the same distance or move towards the MW approaching the present day. However, many satellites with long or unidentified orbital periods (pink

circles) redistribute by tens of kiloparsecs in the last billion years. Nearly twice as many of these satellites fall above the one-to-one relation at $D \sim 25 - 150$ kpc than below it in the same distance range. The former are the satellites moving towards the MW, which includes the LMC and its companion satellites, while the latter are those moving away from the MW.

The changes between radial profiles at 2 Gyr ago and 1 Gyr ago (gray line in the bottom panel of Figure 1) are more gradual but persist across nearly the entire 300 kpc distance range. The right panel of Figure 5 shows the distances of all satellites at 1 Gyr ago (D_1) versus 2 Gyr ago (D_2), classified by the length of the orbital period.

Comparing D_2 and D_1 , 28% of satellites are in the gray-shaded region, where distances have not changed by more than ± 15 kpc. These are primarily satellites with short or intermediate-length orbital periods. However, 52% of satellites have $D_2 - D_1 > +15$ kpc. Thus, most satellites are approaching the MW today, while only 14% are moving away from the MW ($D_2 - D_1 > -15$ kpc). These trends explain the gradually changing gray differential in the bottom left panel of Figure 1, where the satellites moving towards the MW contribute

to where ΔN_{sat} is the smallest at $D = 25 - 125$ kpc. In contrast, the smaller fraction of satellites moving away from the MW gives rise to the changes in the differential at $D > 125$ kpc.

In contrast to the bottom left panel of Figure 1, the bottom right panel of Figure 1 shows the magnitude of $\Delta N_{\text{sat}}(< D)$ is relatively constant over time. Changes in the differential radial profiles are most significant between $D = 25 - 75$ kpc. Between present-day and 1 Gyr ago, seven satellites with long period orbits move toward the MW from $D_1 \sim 75 - 150$ to $D_0 = 25 - 75$

kpc. This shift of satellites toward the inner MW halo corresponds to the changes in the black differential in the bottom right panel of Figure 1 between $D = 25 - 75$ kpc.

These satellites on long-period orbits moving toward the MW also give rise to the sharp increase of satellites in the cumulative radial profiles at present-day distances of $D \sim 25 - 75$ kpc in both bottom panels of Figure 1. Similarly, they also affect the evolution of R_{50} , as shown in Figure 2, such that R_{50} steadily declines between 1 Gyr and today in the rigid MW+LMC potential and from 0.5 Gyr to present day for the rigid MW potential.

REFERENCES

- Astropy Collaboration, Robitaille, T. P., Tollerud, E. J., et al. 2013, *aap*, 558, A33, doi: [10.1051/0004-6361/201322068](https://doi.org/10.1051/0004-6361/201322068)
- Astropy Collaboration, Price-Whelan, A. M., Lim, P. L., et al. 2022, *ApJ*, 935, 167, doi: [10.3847/1538-4357/ac7c74](https://doi.org/10.3847/1538-4357/ac7c74)
- Battaglia, G., Taibi, S., Thomas, G. F., & Fritz, T. K. 2022, *A&A*, 657, A54, doi: [10.1051/0004-6361/202141528](https://doi.org/10.1051/0004-6361/202141528)
- Belokurov, V., Erkal, D., Evans, N. W., Koposov, S. E., & Deason, A. J. 2018, *MNRAS*, 478, 611, doi: [10.1093/mnras/sty982](https://doi.org/10.1093/mnras/sty982)
- Benisty, D. 2024, *A&A*, 689, L1, doi: [10.1051/0004-6361/202449884](https://doi.org/10.1051/0004-6361/202449884)
- Benisty, D., Vasiliev, E., Evans, N. W., et al. 2022, *ApJL*, 928, L5, doi: [10.3847/2041-8213/ac5c42](https://doi.org/10.3847/2041-8213/ac5c42)
- Bennet, P., Sand, D. J., Crnojević, D., et al. 2019, *ApJ*, 885, 153, doi: [10.3847/1538-4357/ab46ab](https://doi.org/10.3847/1538-4357/ab46ab)
- . 2020, *ApJL*, 893, L9, doi: [10.3847/2041-8213/ab80c5](https://doi.org/10.3847/2041-8213/ab80c5)
- Bennet, P., Patel, E., Sohn, S. T., et al. 2024, *ApJ*, 971, 98, doi: [10.3847/1538-4357/ad5349](https://doi.org/10.3847/1538-4357/ad5349)
- Besla, G., Kallivayalil, N., Hernquist, L., et al. 2007, *ApJ*, 668, 949, doi: [10.1086/521385](https://doi.org/10.1086/521385)
- Buch, D., Nadler, E. O., Wechsler, R. H., & Mao, Y.-Y. 2024, *arXiv e-prints*, arXiv:2404.08043, doi: [10.48550/arXiv.2404.08043](https://doi.org/10.48550/arXiv.2404.08043)
- Carlsten, S. G., Greene, J. E., Beaton, R. L., Danieli, S., & Greco, J. P. 2022, *ApJ*, 933, 47, doi: [10.3847/1538-4357/ac6fd7](https://doi.org/10.3847/1538-4357/ac6fd7)
- Chamberlain, K., Price-Whelan, A. M., Besla, G., et al. 2022, *arXiv e-prints*, arXiv:2204.07173, <https://arxiv.org/abs/2204.07173>
- Crnojević, D., Sand, D. J., Bennet, P., et al. 2019, *ApJ*, 872, 80, doi: [10.3847/1538-4357/aafbe7](https://doi.org/10.3847/1538-4357/aafbe7)
- Danieli, S., van Dokkum, P., Merritt, A., et al. 2017, *ApJ*, 837, 136, doi: [10.3847/1538-4357/aa615b](https://doi.org/10.3847/1538-4357/aa615b)
- Erkal, D., & Belokurov, V. A. 2020, *MNRAS*, 495, 2554, doi: [10.1093/mnras/staa1238](https://doi.org/10.1093/mnras/staa1238)
- Erkal, D., Deason, A. J., Belokurov, V., et al. 2021, *MNRAS*, 506, 2677, doi: [10.1093/mnras/stab1828](https://doi.org/10.1093/mnras/stab1828)
- Fritz, T. K., Battaglia, G., Pawlowski, M. S., et al. 2018, *A&A*, 619, A103, doi: [10.1051/0004-6361/201833343](https://doi.org/10.1051/0004-6361/201833343)
- Garavito-Camargo, N., Besla, G., Laporte, C. F. P., et al. 2019, *ApJ*, 884, 51, doi: [10.3847/1538-4357/ab32eb](https://doi.org/10.3847/1538-4357/ab32eb)
- . 2021, *ApJ*, 919, 109, doi: [10.3847/1538-4357/ac0b44](https://doi.org/10.3847/1538-4357/ac0b44)
- Garrison-Kimmel, S., Wetzel, A., Bullock, J. S., et al. 2017, *MNRAS*, 471, 1709, doi: [10.1093/mnras/stx1710](https://doi.org/10.1093/mnras/stx1710)
- Garrison-Kimmel, S., Hopkins, P. F., Wetzel, A., et al. 2019, *MNRAS*, 487, 1380, doi: [10.1093/mnras/stz1317](https://doi.org/10.1093/mnras/stz1317)
- Geha, M., Wechsler, R. H., Mao, Y.-Y., et al. 2017, *ApJ*, 847, 4, doi: [10.3847/1538-4357/aa8626](https://doi.org/10.3847/1538-4357/aa8626)
- Griffen, B. F., Ji, A. P., Dooley, G. A., et al. 2016, *ApJ*, 818, 10, doi: [10.3847/0004-637X/818/1/10](https://doi.org/10.3847/0004-637X/818/1/10)
- Harris, C. R., Millman, K. J., van der Walt, S. J., et al. 2020, *Nature*, 585, 357, doi: [10.1038/s41586-020-2649-2](https://doi.org/10.1038/s41586-020-2649-2)
- Helmi, A., Babusiaux, C., Koppelman, H. H., et al. 2018, *Nature*, 563, 85, doi: [10.1038/s41586-018-0625-x](https://doi.org/10.1038/s41586-018-0625-x)
- Hunter, J. D. 2007, *Computing in Science Engineering*, 9, 90, doi: [10.1109/MCSE.2007.55](https://doi.org/10.1109/MCSE.2007.55)
- Jethwa, P., Erkal, D., & Belokurov, V. 2016, *MNRAS*, 461, 2212, doi: [10.1093/mnras/stw1343](https://doi.org/10.1093/mnras/stw1343)
- Kallivayalil, N., van der Marel, R. P., Besla, G., Anderson, J., & Alcock, C. 2013, *ApJ*, 764, 161, doi: [10.1088/0004-637X/764/2/161](https://doi.org/10.1088/0004-637X/764/2/161)
- Kelley, T., Bullock, J. S., Garrison-Kimmel, S., et al. 2019, *MNRAS*, 487, 4409, doi: [10.1093/mnras/stz1553](https://doi.org/10.1093/mnras/stz1553)
- Kluyver, T., Ragan-Kelley, B., Pérez, F., et al. 2016, in *Positioning and Power in Academic Publishing: Players, Agents and Agendas*, ed. F. Loizides & B. Schmidt, IOS Press, 87 – 90
- Kondapally, R., Russell, G. A., Conselice, C. J., & Penny, S. J. 2018, *MNRAS*, 481, 1759, doi: [10.1093/mnras/sty2333](https://doi.org/10.1093/mnras/sty2333)

- Kravtsov, A., & Winney, S. 2024, arXiv e-prints, arXiv:2405.06017, doi: [10.48550/arXiv.2405.06017](https://doi.org/10.48550/arXiv.2405.06017)
- Law, D. R., Johnston, K. V., & Majewski, S. R. 2005, ApJ, 619, 807, doi: [10.1086/426779](https://doi.org/10.1086/426779)
- Libeskind, N. I., Frenk, C. S., Cole, S., et al. 2005, MNRAS, 363, 146, doi: [10.1111/j.1365-2966.2005.09425.x](https://doi.org/10.1111/j.1365-2966.2005.09425.x)
- Lilleengen, S., Petersen, M. S., Erkal, D., et al. 2023, MNRAS, 518, 774, doi: [10.1093/mnras/stac3108](https://doi.org/10.1093/mnras/stac3108)
- Mao, Y.-Y., Geha, M., Wechsler, R. H., et al. 2021, ApJ, 907, 85, doi: [10.3847/1538-4357/abce58](https://doi.org/10.3847/1538-4357/abce58)
- Mao, Y.-Y., Williamson, M., & Wechsler, R. H. 2015, ApJ, 810, 21, doi: [10.1088/0004-637X/810/1/21](https://doi.org/10.1088/0004-637X/810/1/21)
- Mao, Y.-Y., Geha, M., Wechsler, R. H., et al. 2024, arXiv e-prints, arXiv:2404.14498, doi: [10.48550/arXiv.2404.14498](https://doi.org/10.48550/arXiv.2404.14498)
- McConnachie, A. W. 2012, AJ, 144, 4, doi: [10.1088/0004-6256/144/1/4](https://doi.org/10.1088/0004-6256/144/1/4)
- McConnachie, A. W., & Venn, K. A. 2020a, AJ, 160, 124, doi: [10.3847/1538-3881/aba4ab](https://doi.org/10.3847/1538-3881/aba4ab)
- . 2020b, Research Notes of the American Astronomical Society, 4, 229, doi: [10.3847/2515-5172/abd18b](https://doi.org/10.3847/2515-5172/abd18b)
- McMillan, P. J. 2017, MNRAS, 465, 76, doi: [10.1093/mnras/stw2759](https://doi.org/10.1093/mnras/stw2759)
- Nadler, E. O., Wechsler, R. H., Bechtol, K., et al. 2020, ApJ, 893, 48, doi: [10.3847/1538-4357/ab846a](https://doi.org/10.3847/1538-4357/ab846a)
- Nadler, E. O., Mansfield, P., Wang, Y., et al. 2023, ApJ, 945, 159, doi: [10.3847/1538-4357/acb68c](https://doi.org/10.3847/1538-4357/acb68c)
- Patel, E., Besla, G., & Mandel, K. 2017b, MNRAS, 468, 3428, doi: [10.1093/mnras/stx698](https://doi.org/10.1093/mnras/stx698)
- Patel, E., Besla, G., Mandel, K., & Sohn, S. T. 2018, ApJ, 857, 78, doi: [10.3847/1538-4357/aab78f](https://doi.org/10.3847/1538-4357/aab78f)
- Patel, E., Besla, G., & Sohn, S. T. 2017, MNRAS, 464, 3825, doi: [10.1093/mnras/stw2616](https://doi.org/10.1093/mnras/stw2616)
- Patel, E., & Mandel, K. S. 2022, arXiv e-prints, arXiv:2211.15928, doi: [10.48550/arXiv.2211.15928](https://doi.org/10.48550/arXiv.2211.15928)
- Patel, E., Kallivayalil, N., Garavito-Camargo, N., et al. 2020, ApJ, 893, 121, doi: [10.3847/1538-4357/ab7b75](https://doi.org/10.3847/1538-4357/ab7b75)
- Pawlowski, M. S., & Kroupa, P. 2019, MNRAS, 2774, doi: [10.1093/mnras/stz3163](https://doi.org/10.1093/mnras/stz3163)
- Perez, F., & Granger, B. E. 2007, Computing in Science Engineering, 9, 21, doi: [10.1109/MCSE.2007.53](https://doi.org/10.1109/MCSE.2007.53)
- Price-Whelan, A. M. 2017, The Journal of Open Source Software, 2, doi: [10.21105/joss.00388](https://doi.org/10.21105/joss.00388)
- Price-Whelan, A. M., Sip'ocz, B. M., G'unther, H. M., et al. 2018, aj, 156, 123, doi: [10.3847/1538-3881/aabc4f](https://doi.org/10.3847/1538-3881/aabc4f)
- Richstein, H., Patel, E., Kallivayalil, N., et al. 2022, ApJ, 933, 217, doi: [10.3847/1538-4357/ac7226](https://doi.org/10.3847/1538-4357/ac7226)
- Sales, L. V., Navarro, J. F., Kallivayalil, N., & Frenk, C. S. 2017, MNRAS, 465, 1879, doi: [10.1093/mnras/stw2816](https://doi.org/10.1093/mnras/stw2816)
- Samuel, J., Wetzel, A., Chapman, S., et al. 2021, MNRAS, 504, 1379, doi: [10.1093/mnras/stab955](https://doi.org/10.1093/mnras/stab955)
- Samuel, J., Wetzel, A., Santistevan, I., et al. 2022, MNRAS, 514, 5276, doi: [10.1093/mnras/stac1706](https://doi.org/10.1093/mnras/stac1706)
- Samuel, J., Wetzel, A., Tollerud, E., et al. 2020, MNRAS, 491, 1471, doi: [10.1093/mnras/stz3054](https://doi.org/10.1093/mnras/stz3054)
- Santistevan, I. B., Wetzel, A., Tollerud, E., et al. 2024, MNRAS, 527, 8841, doi: [10.1093/mnras/stad3757](https://doi.org/10.1093/mnras/stad3757)
- Santistevan, I. B., Wetzel, A., Tollerud, E., Sanderson, R. E., & Samuel, J. 2023, MNRAS, 518, 1427, doi: [10.1093/mnras/stac3100](https://doi.org/10.1093/mnras/stac3100)
- Shipp, N., Erkal, D., Drlica-Wagner, A., et al. 2021, ApJ, 923, 149, doi: [10.3847/1538-4357/ac2e93](https://doi.org/10.3847/1538-4357/ac2e93)
- Simon, J. D. 2019, ARA&A, 57, 375, doi: [10.1146/annurev-astro-091918-104453](https://doi.org/10.1146/annurev-astro-091918-104453)
- Smercina, A., Bell, E. F., Price, P. A., et al. 2018, ApJ, 863, 152, doi: [10.3847/1538-4357/aad2d6](https://doi.org/10.3847/1538-4357/aad2d6)
- Sohn, S. T., Besla, G., van der Marel, R. P., et al. 2013, ApJ, 768, 139, doi: [10.1088/0004-637X/768/2/139](https://doi.org/10.1088/0004-637X/768/2/139)
- Sohn, S. T., Patel, E., Fardal, M. A., et al. 2020, ApJ, 901, 43, doi: [10.3847/1538-4357/abaf49](https://doi.org/10.3847/1538-4357/abaf49)
- Sohn, S. T., Patel, E., Besla, G., et al. 2017, ApJ, 849, 93, doi: [10.3847/1538-4357/aa917b](https://doi.org/10.3847/1538-4357/aa917b)
- Spencer, M., Loebman, S., & Yoachim, P. 2014, ApJ, 788, 146, doi: [10.1088/0004-637X/788/2/146](https://doi.org/10.1088/0004-637X/788/2/146)
- van der Marel, R. P., Fardal, M., Besla, G., et al. 2012, ApJ, 753, 8, doi: [10.1088/0004-637X/753/1/8](https://doi.org/10.1088/0004-637X/753/1/8)
- . 2012a, ApJ, 753, 8, doi: [10.1088/0004-637X/753/1/8](https://doi.org/10.1088/0004-637X/753/1/8)
- van der Marel, R. P., Fardal, M. A., Sohn, S. T., et al. 2019, ApJ, 872, 24, doi: [10.3847/1538-4357/ab001b](https://doi.org/10.3847/1538-4357/ab001b)
- van der Marel, R. P., & Kallivayalil, N. 2014, ApJ, 781, 121, doi: [10.1088/0004-637X/781/2/121](https://doi.org/10.1088/0004-637X/781/2/121)
- Vasiliev, E. 2023, Galaxies, 11, 59, doi: [10.3390/galaxies11020059](https://doi.org/10.3390/galaxies11020059)
- Virtanen, P., Gommers, R., Oliphant, T. E., et al. 2020, Nature Methods, 17, 261, doi: [10.1038/s41592-019-0686-2](https://doi.org/10.1038/s41592-019-0686-2)
- Wang, Y., Nadler, E. O., Mao, Y.-Y., et al. 2024, arXiv e-prints, arXiv:2404.14500, doi: [10.48550/arXiv.2404.14500](https://doi.org/10.48550/arXiv.2404.14500)
- Watkins, L. L., van der Marel, R. P., & Bennet, P. 2024, ApJ, 963, 84, doi: [10.3847/1538-4357/ad1f58](https://doi.org/10.3847/1538-4357/ad1f58)